Journal of Power Sources 196 (2011) 8398–8401

Contents lists available at ScienceDirect

Journal of Power Sources

journal homepage: www.elsevier.com/locate/jpowsour

Short communication

Fuel crossover and internal current in polymer electrolyte membrane fuel cell from water visualization using X-ray radiography

Jongrok Kim[a], Junho Je[a], Massoud Kaviany[b,d], Sang Young Son[c], MooHwan Kim[d,*]

[a] Department of Mechanical Engineering, Pohang University of Science and Technology, San 31, Hyoja-dong, Namgu, Pohang, Kyoungbuk 790-784, South Korea
[b] Department of Mechanical Engineering, University of Michigan, Ann Arbor, MI 48109-2125, USA
[c] School of Dynamic Systems, University of Cincinnati, Cincinnati, OH 45221, USA
[d] Division of Advanced Nuclear Engineering, Pohang University of Science and Technology, San 31, Hyoja-dong, Namgu, Pohang, Kyoungbuk 790-784, South Korea

ARTICLE INFO

Article history:
Received 9 March 2011
Received in revised form 18 May 2011
Accepted 27 May 2011
Available online 23 June 2011

Keywords:
Polymer electrolyte membrane fuel cell
Fuel crossover
Internal current
Open-circuit voltage
X-ray radiography

ABSTRACT

The fuel crossover and internal current in a polymer electrolyte membrane fuel cell undergo a chemical reaction in the cell without power generation. These are the main phenomena for reduced cell voltage at low current density. This fuel crossover also degrades the fuel cell performance, efficiency, and durability. Thus, observation of these phenomena is important for understanding and developing a polymer electrolyte membrane fuel cell. Using X-ray radiography, the water distribution and membrane swelling, which indicate fuel crossover and internal current, in an operating polymer electrolyte membrane fuel cell under open-circuit conditions were examined. The X-ray images effectively demonstrated the transient changes of each phenomenon, which are related to the properties of each component and the operating conditions.

1. Introduction

Fuel cells are electrochemical devices that directly convert the bond energy of reactants into electricity and heat. The polymer electrolyte membrane (PEM) fuel cell uses a solid-state proton-conducting polymer membrane as the electrolyte. Theoretically, a PEM fuel cell has an open-circuit voltage (OCV) of 1.2 V (for a cell operating below 100 °C), but during operation, the OCV is approximately 1.0 V [1]. The internal current (1 mA cm^{-2} [1]) and fuel crossover, which flow from the anode to the cathode through the membrane, cause this voltage drop. Although the membrane is electrically nonconductive and practically impermeable to reactant gases, some electrons may find a shortcut through the membrane, and small amounts of hydrogen will diffuse from the anode to the cathode. When a fuel cell is operated under open-circuit or very low current density conditions, these losses may have a marked effect on the cell potential [1,2]. Additionally, fuel crossover degrades fuel cell performance, efficiency, and durability. The fuel crossover causes direct combustion of hydrogen and oxygen in the catalyst layer, and this generates a local hot spot that causes pinholes, initiating a destructive cycle of increased crossover and membrane degradation [3]. Fuel crossover also generates hydrogen peroxide, which can cause chemical degradation [4]. Thus, an analysis of fuel crossover and the internal current is important for the development of membranes. The rate of fuel crossover through the membrane has been measured using linear sweep voltammetry [5,6] and chronocoulometry [7]; however, these methods measure the fuel crossover rate under non-operating conditions because they require H_2 and N_2.

The aim of this study was to visualize the changes caused by fuel crossover and internal current in a PEM fuel cell under operating conditions with H_2 and air. X-ray radiography was used for the visualization. This technique has been applied to visualize the internal structure and water distribution in PEM fuel cells [8–13] because it can be used to observe phenomena in a fuel cell that has not been modified for visualization under operating conditions.

2. Experimental methods

Each single fuel cell (Fig. 1) had a 2 cm × 2 cm active area, and consisted of an anode bipolar plate with a serpentine channel, a cathode bipolar plate with nine holes to supply ambient air (about 23 °C), two gas diffusion layers (GDLs; Toray TGPH-090), and a membrane electrode assembly (MEA), which consisted of Gore Primea MEAs for transportation and had two catalyst layers (cathode Pt loading: 0.4 mg cm^{-2}, anode Pt loading: 0.1 mg cm^{-2}). Components were assembled between two polymer endplates with four bolts and compression force was controlled using a torque

* Corresponding author. Tel.: +82 54 279 2165; fax: +82 54 279 3199.
E-mail address: mhkim@postech.ac.kr (M. Kim).

0378-7753/$ – see front matter © 2011 Elsevier B.V. All rights reserved.
doi:10.1016/j.jpowsour.2011.05.072

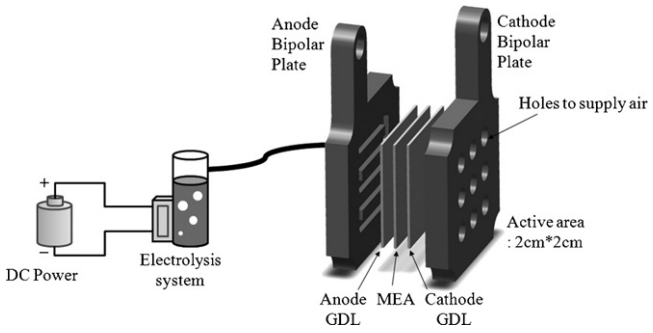

Fig. 1. PEM fuel cell and electrolysis system.

wrench. An electrolysis system was used to produce hydrogen gas; its flow rate was $7.1 \pm 1.1\ \mathrm{mL\,min^{-1}}$, the temperature was 23.5 °C, and the relative humidity was 97%, so the vapor in the gas could condense in the fuel cell. To verify the condensation effect of this vapor, another fuel cell that had a membrane (Nafion N212) with no catalyst layer was also tested. After operating a fuel cell, there is a potential for liquid water to remain, even after it has been desiccated. For this reason, each experiment was conducted using a new membrane and GDLs. To avoid external electric current, which flows through the external load, voltage and current measurement systems were not used.

Each single fuel cell was analyzed with an X-ray microscope system at the Pohang Accelerator Laboratory, Pohang University of Science and Technology, Korea (Fig. 2). The incident white X-ray beam (photon energy 2.8–5.5 keV) passed through the sample and reached a scintillator that converted the X-rays to visible rays. The visible rays were reflected off a mirror through a microscope into a 16-bit 4008 × 2672-pixel charge-coupled-device (CCD) camera. The field of view was 5.05 mm × 3.36 mm.

To analyze these phenomena, the water thickness is an important parameter. The calculation processing step for water thickness was as follows [14,15]. First, dividing the gray value of the ***wet*** image by the gray value of the ***dry*** image and using a negative natural log to obtain the value of μt

$$T = -\ln\left(\frac{\Phi_{wet}}{\Phi_{Dry}}\right) = -\ln\left[\frac{\Phi_o \exp\left(-\sum_i \mu_i t_i - \mu_{water} t_{water}\right)}{\Phi_o \exp\left(-\sum_i \mu_i t_i\right)}\right] = \mu_{water} t_{water} \quad (1)$$

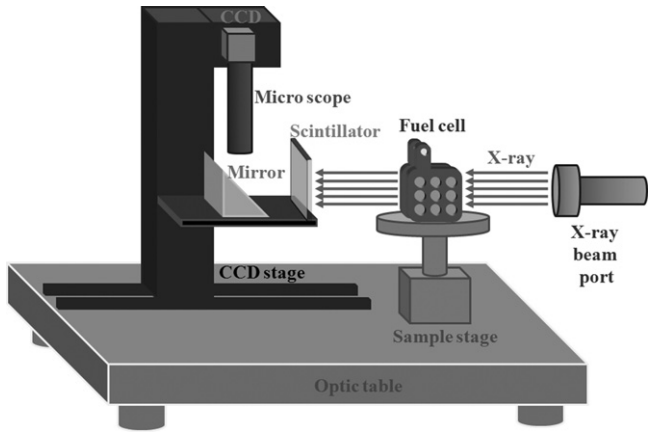

Fig. 2. Fuel cell and the X-ray microscope and beamline at the Pohang Accelerator Laboratory.

Then, the water thickness or volume can be calculated with the linear attenuation coefficient μ of water that is measured experimentally:

$$t_{water} = \frac{T}{\mu_{water}} \quad (2)$$

A calibration step was applied to measure the linear attenuation coefficient of water. The measured value was $19.169\ \mathrm{cm^{-1}}$.

3. Results and discussion

The MEA and membrane have higher attenuation coefficients compared with that of the GDL. Thus, they appear darker than the GDL in X-ray images (Fig. 3). One hundred X-ray images were continuously recorded for 400 s, which was the duration of experiments. The images in Fig. 3 are for the initial stage and 380 s after experiments begun, when the MEA thickness and water thickness in the GDL had reached a steady state. Although the MEA thickness was 35 μm, the membrane (N212) was 50 μm, and GDL (TGPH-090) was 280 μm, the thickness of the MEA and the membrane in Fig. 3 appear thicker than the true value. The cells were arranged with all components in parallel; however, it is difficult to make them exactly parallel. Thus, the interfaces overlapped and there is not a sharp interface. For this reason, relative thickness changes only were analyzed. The membrane thickness of the fuel cell with catalyst layers increased after hydrogen injection, whereas there was no change in the fuel cell without catalyst layers (Fig. 3). The gray values of the X-ray images were plotted for a detailed comparison (Figs. 4 and 5). The gray values in the image of the fuel cell containing catalyst layers (Fig. 4) showed that the membrane swelled and water was produced in the cathode GDL near the membrane. The gray value in the cathode GDL region decreased because the liquid water produced, which had a higher attenuation coefficient than air, filled the pores in the GDL, and this liquid water absorbed X-rays. For the fuel cell with no catalyst layer, the gray values before and after the hydrogen gas supply were identical (Fig. 5), indicating that there was no condensed water effect.

The swelling of the MEA and increase in the water thickness in the GDL were caused by the water. Generally, electrons are separated on an anode catalyst layer and move to the cathode catalyst layer along an external load. Then, they are combined with protons and oxygen, producing water via a chemical reaction. In this experiment, however, the produced water existed even though there was no external channel for electrons. There are two possible explanations for this observation. In the first scenario, electrons and protons that are separated in the anode catalyst layer combine with the residual air in the anode channel. In this case, water is produced on the anode side and accumulates in the anode GDL. A second possible explanation is the existence of hydrogen crossover and an internal current. If there is crossover of hydrogen gas, the chemical reaction would occur only in the cathode catalyst layer and water would be produced there. If there is an internal current, the electrons and protons that are separated in the anode catalyst layer move through the membrane at once. Based on the experimental results, there was no water in the anode GDL, indicating that there was no significant direct reaction in the anode side. Thus, the first scenario did not occur and the second possibility does explain the changes observed in the cell. That is, the MEA swelling and increased water thickness in the GDL were apparently caused by the crossover of hydrogen gas and an internal current.

The rate of change of MEA thickness and water thickness in the cathode GDL were also calculated (Fig. 5) from X-ray images recorded during the experiment. The MEA thickness was used to calculate the number of pixels under the threshold value, which was 6000. The water thickness in the GDL was calculated as described in the previous section. The increased MEA thickness and

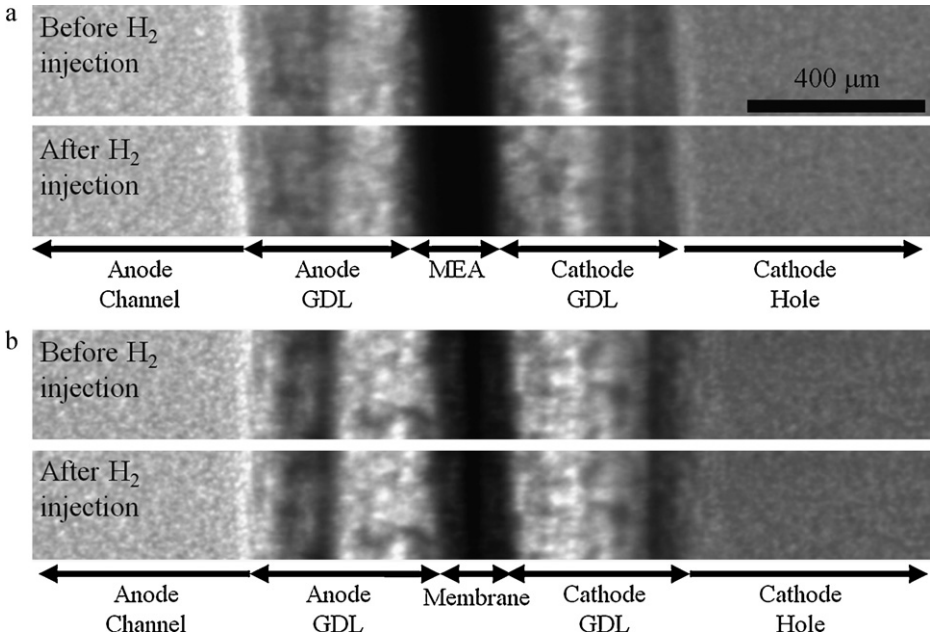

Fig. 3. X-ray images before and after hydrogen gas injection, for (a) the membrane with a catalyst layer, and (b) the membrane without a catalyst layer.

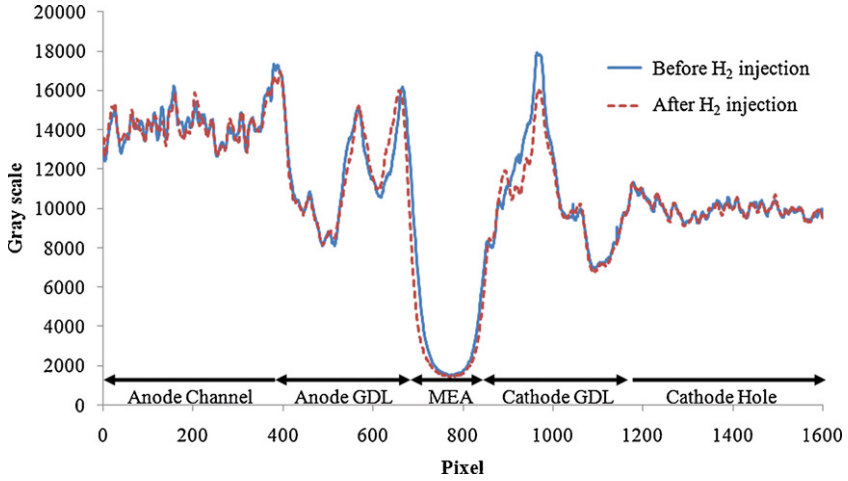

Fig. 4. Gray-scale distributions of X-ray recording before and after hydrogen gas injection, with the MEA present.

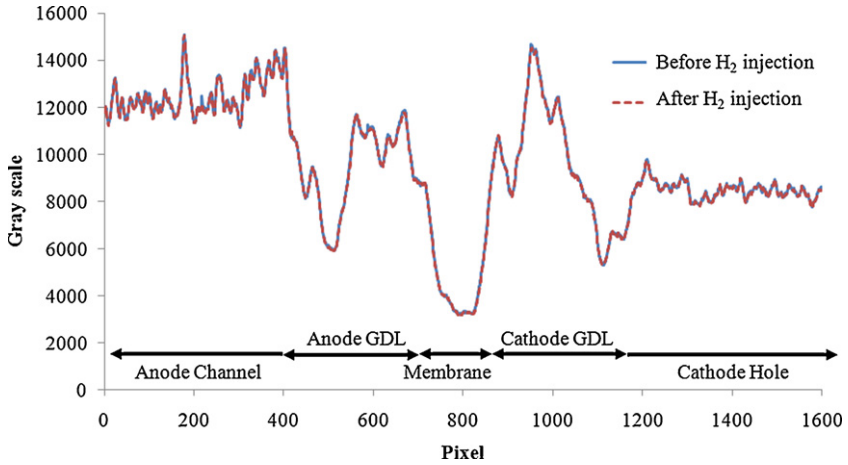

Fig. 5. Gray-scale distributions of X-ray recording before and after hydrogen gas injection with no catalyst layer.

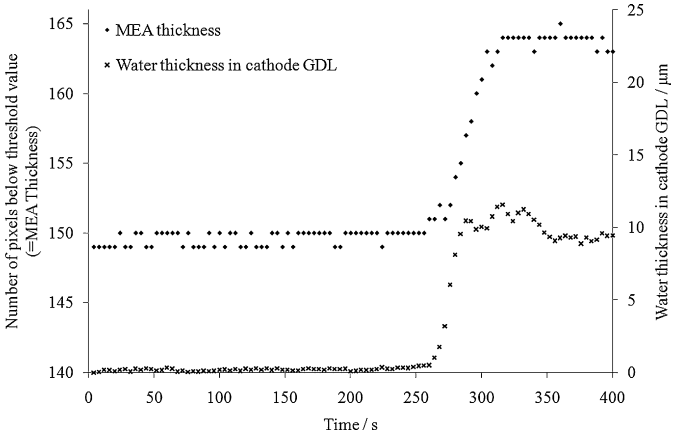

Fig. 6. Measured variations of the MEA thickness (upper curve) and water thickness on the cathode GDL (lower curve) over time.

water thickness in the cathode GDL began at the same time, but the MEA thickness took longer to reach the steady state compared with the water thickness in the cathode GDL (Fig. 6). This difference in rates in the MEA and GDL is related to the properties of the MEA and GDL; it also depends on the experimental conditions because the gas permeability of the membrane changes with the temperature and water content [5], and the permeability affects the rate of chemical reaction in the catalyst layer. A parametric study is required to verify this relationship.

4. Conclusions

In this study, X-ray radiography was used to visualize the phenomena that are caused by fuel crossover and internal current through the membrane in a PEM fuel cell under open-circuit conditions. X-ray images effectively demonstrated transient changes by these phenomena in a PEM fuel cell. After hydrogen gas injection into the anode side, the membrane swelled (increased membrane water content), and the liquid water produced was observed in the cathode GDL. The MEA and GDL require different lengths of time to reach steady state; this rate is dependent on the properties of each component and the operating conditions. A parametric study is required to verify this relationship.

Acknowledgements

This research was supported by the World Class University (WCU) program through the National Research Foundation of Korea, funded by the Ministry of Education, Science and Technology (R31-30005), and the National Research Foundation of Korea (NRF), through a grant provided by the Korean Ministry of Science and Technology (MOST), M60602000005-06E0200-00410.

References

[1] J. Larminie, A. Dick, Fuel Cell Systems Explained, John Wiley & Sons Ltd., Chichester, England, 2003.
[2] F. Barbir, PEM Fuel Cells: Theory and Practice, Elsevier Academic Press, New York, 2005, p. 42.
[3] J. Zhang, Z. Xie, J. Zhang, Y. Tang, C. Song, T. Navessin, Z. Shi, D. Song, H. Wang, D.P. Wilkinson, Z.-S. Liu, S. Holdcroft, High temperature PEM fuel cells, J. Power Sources 160 (2) (2006) 872.
[4] M. Inaba, T. Kinumoto, M. Kiriake, R. Umebayashi, A. Tasaka, Z. Ogumib, Gas crossover and membrane degradation in polymer electrolyte fuel cells, Electrochim. Acta 51 (2006) 5746.
[5] S.S. Kocha, J.D. Yang, J.S. Yi, Characterization of gas crossover and its implications in PEM fuel cells, Am. Inst. Chem. Eng. 52 (5) (2006) 1916.
[6] Y. Song, J.M. Fenton, H.R. Kunz, L.J. Bonville, M.V. Williams, High-performance PEMFCs at elevated temperatures using Nafion 112 membranes, J. Electrochem. Soc. 152 (3) (2005) A539.
[7] J. Yu, T. Matsuura, Y. Yoshikawa, M.N. Islam, M. Hori, In situ analysis of performance degradation of a PEMFC under nonsaturated humidification, Electrochem. Solid-State Lett. 8 (3) (2005) A156.
[8] P.K. Sinha, P. Halleck, C.-Y. Wang, Quantification of liquid water saturation in a PEM fuel cell diffusion medium using X-ray microtomography, Electrochem. Solid-State Lett. 9 (7) (2006) A344.
[9] F.N. Büchia, R. Flückigera, D. Tehlara, F. Maroneb, M. Stampanonib, Determination of liquid water distribution in porous transport layers, ECS Trans. 16 (2) (2008) 587.
[10] C. Hartnig, I. Manke, R. Kuhn, N. Kardjilov, J. Banhart, W. Lehnert, Cross-sectional insight in the water evolution and transport in polymer electrolyte fuel cells, Appl. Phys. Lett. 92 (2008) 134106.
[11] C. Harting, I. Manke, R. Kuhn, S. Kleinau, J. Goebbels, J. Banhart, High-resolution in-plane investigation of the water evolution and transport in PEM fuel cells, J. Power Sources 188 (2009) 468.
[12] S.J. Lee, S.G. Kim, G.G. Park, C.S. Kim, Quantitative visualization of temporal water evolution in an operating polymer electrolyte fuel cell, Int. J. Hydrogen Energy 35 (19) (2010) 10457.
[13] S. Tsushima, S. Hirai, In situ diagnostics for water transport in proton exchange membrane fuel cells, Prog. Energy Combust. Sci. 37 (2) (2011) 204.
[14] D.J. Ludlow, C.M. Calebrese, S.H. Yu, C.S. Dannehy, D.L. Jacobson, D.S. Hussey, M. Arif, M.K. Jensen, G.A. Eisman, PEM fuel cell membrane hydration measurement by neutron imaging, J. Power Sources 162 (2006) 271.
[15] T.J. Kim, J. Kim, C.M. Sim, S.H. Lee, Y.J. Son, M.H. Kim, Experimental approaches for discharge characteristics in PEMFC using neutron imaging technique at CONRAD, HMI, Nucl. Eng. Technol. 41 (1) (2009) 135.